This article has been accepted for publication in a future issue of this journal, but has not been fully edited. Content may change prior to final publication. Citation information: DOI 10.1109/TSG.2016.2548082, IEEE Transactions on Smart Grid

A New Dynamic Performance Model of Motor Stalling and FIDVR for Smart Grid Monitoring/Planning

Honghao Zheng, *Member, IEEE,* Christopher L. DeMarco, *Member, IEEE,*

***Abstract*—The stalling of highly concentrated constant torque induction motor loads due to system faults may result in fault induced delayed voltage recovery (FIDVR). This state can cause significantly depressed local voltage for several seconds after the fault is cleared, and can also lead to widely cascaded system failure. Though there is extensive study conducted within the modeling of motor loads, the dynamic connection between the aggregated induction motor loads and the grid still needs further investigation. In this work, a dynamic performance model is developed for motor stalling and over heat thermal tripping. Specifically, this dynamic model can be constructed with an energy-like Lyapunov function, and can be incorporated as part of power system dynamic cascading model. The simulation examples are carried out in an enhanced version of the IEEE 57 bus test system, as demonstration for feasibility. This model may be beneficiary for smart grid monitoring and planning, as well as energy analysis for power system cascading failure.**

***Index Terms*—Motor Stalling, Fault Induced Delayed Voltage Recovery, Power System Cascading Failure, Energy-like Lyapunov Function**

I. Introduction

In a distribution network with a high concentration of induction motors driving mechanical compressor loads (most notably, air conditioners), a fault-induced, temporary low voltage may cause some of these induction motors to stall. These stalled units draw large amount of reactive power, and further depress local voltage for several seconds after the fault is cleared. The local voltage may gradually recover, and often exceeds its value at the normal operating point, because many of the stalled units will trip themselves off the grid by action of thermal protection having an inverse time-over current characteristic, which can take from 3 to 20 seconds [1]. This phenomenon is usually referred as fault-induced delayed voltage recovery (FIDVR). As the description above suggests, a system experiencing FIDVR is vulnerable to more widespread cascading failure, depending on the speed with which thermal relays act. If a system is experiencing depressed voltage, then any additional fault during the interval may result in further stalling of motor on other nearby feeders, and may result in a cascade in which growing numbers of motors stall, with ultimately collapsing voltage (i.e., no voltage recovery) [2]. Figure 1 illustrates the phenomenon with a representative voltage versus time plot.

This work is supported in part by a contract from Argonne, a U.S. Department of Energy Office of Science Laboratory, and was sponsored by the Applied Mathematics Activity, Advanced Scientific Computing Research Program within the DOE Office of Science.

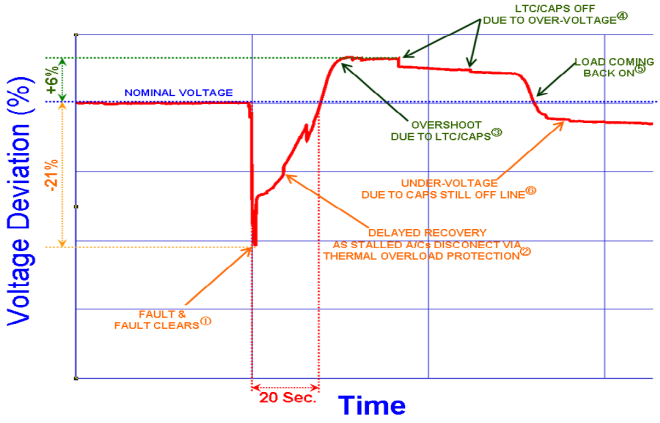

Fig. 1. Illustration of a typical FIDVR scenario following a 230kV transmission line fault in Southern California [1]

Literature studying this class of problems has mainly focused on two aspects: 1) creation of time domain simulation models to represent the motor load in a fashion that accurately replicates field-observed FIDVR phenomenon; 2) how to prevent, and/or mitigate the impact of, induction motor stalling.

Motor models existing in literature can be classified into dynamic phasor models and static performance models. References [3] and [4] well summarize the early work on motor load modeling; here we briefly review publications subsequent to those. Dynamic phasor models are generally proposed based on a reference frame transformation and detailed flux modeling [5], [6]. A recent study developed a set of differential equations to represent single phase induction motor (SPIM) model that can be used in an electro-magnetic transients, and observed the detailed relationship between voltage dip and motor stall [7]. Compared to the dynamic phasor model, the static performance model is constructed from the "grid perspective". In other words, the effects of motor loads is represented in the form of real and reactive power consumption. Static performance models are usually derived based on experiment data [6], [8]. Apart from the deterministic performance model, [9] and [10] modeled the motor stall probabilistically within the CASCADE model to study FIDVR related events.

To mitigate the impact of FIDVR and prevent cascading failure, some researchers have sought best strategy for load shedding [11], while others have designed control schemes for reactive power compenstaion [12].

Though there is extensive work on modeling to represent

This article has been accepted for publication in a future issue of this journal, but has not been fully edited. Content may change prior to final publication. Citation information: DOI 10.1109/TSG.2016.2548082, IEEE Transactions on Smart Grid

motor stall phenomena, such work is largely focused on producing accurate time domain simulations, rather than structural, analytic insights into the system-wide impact of such stalling. Understanding of the interplay between the individual component characteristic (the induction motor stalling) and system-wide phenomena it can induce (cascading failure and voltage collapse) remains worthy of further investigation. In this work, we suggest a new dynamic performance model for motor stalling and tripping, and the incorporation of the component models into an overall system model. In particular, this work will develop an ordinary differential equation model for the power system along with motor stalling, with relay action to disconnect the motors represented as a fast-time scale, but none-the-less smooth phenomena (i.e., the action of the relay very rapidly drive current flow to zero, but does so with current being a smooth function of time). Moreover, this model has a special structure that is closely related to the gradient of a scalar, energy-like function. We show that the time derivative of this energy function along solution trajectories is guaranteed non-positive, and with certain other conditions shown to be satisfied, this may play the role of a Lyapunov function for the system dynamic equations. This specially structured model and its associated Lyapunov function then provides insights into cascading failure analysis [13], as well as power grid dynamic control [14].

The paper is structured as follows: Section II briefly reviews the "system-oriented" classical power system dynamic model and its well-known energy-like Lyapunov function; then the Section III presents the "component-oriented" dynamic performance model for motor under three operating conditions: normal, stall and trip; Section IV then combines these to an overall model that includes the stalling and tripping phenomena, and explores the characteristics of this model in an enhanced version of the IEEE 57 bus test system. Section V demonstrates the application of the energy-like Lyapunov function in visualizing transitions into motor tripping regions (and possible cascading failure) through lower dimensional projections of the energy contours, representing the transition via a "potential boundary" that the system state must overcome to escape from a region of normal operation to a motor-stalled, and ultimately, motor-tripped region of the state space.

II. Power System Dynamic Model and Associated Energy Function

To begin with, let us briefly revisit the classical power system dynamic model. Consider a power system with $N+1$ buses and L branches, with m generator buses, n load buses ($N = m + n$), and a single infinite bus/reference bus. The slack/reference bus is labelled as index 0, followed by indices $1, 2, \cdots, m$ for generator buses, and $m+1, m+2, \cdots, m+n$ for load buses. Transmission lines (and possibly transformer links) are indexed as $1, 2, \cdots, L$.

Then one may define a vector of angle differences relative to the reference bus:

$$\alpha \in \mathbb{R}^N : \alpha_i = \delta_i - \delta_0$$

for $i = 1, 2, \cdots, N$. It is convenient to define $\alpha_0 = \delta_0 - \delta_0 \equiv 0$, recognizing, however, that the constant α_0 does not appear as part of the state variable vector α.

This base system model presented in (1) $\sim$ (3) combines general features of several models in the literature [15], [16], inheriting the form in [17], [18].

$$\dot{\omega}_g = -\mathbf{M}_g^{-1}\mathbf{D}_g\omega_g - \mathbf{M}_g^{-1}\mathbf{\Pi}_1^T f(\alpha, V_l) \tag{1}$$

$$\dot{\alpha} = \mathbf{\Pi}_1\omega_g - [\mathbf{\Pi}_2\mathbf{D}_l^{-1}\mathbf{\Pi}_2^T]f(\alpha, V_l) \tag{2}$$

$$\dot{V}_l = -\mathbf{D}_v^{-1}g(\alpha, V_l) \tag{3}$$

where $V_l = [V_{m+1}, V_{m+2}, \cdots, V_{m+n}]^T$ as load voltage vector. The magnitude of generator buses $V_0, V_1, \cdots, V_m$ is set to constant. Besides,

$$f_i(\alpha, V_l) = V_i \sum_{k=0}^{N} V_k \mathbf{B}_{ik} \sin(\alpha_i - \alpha_k) - P_i^0 \tag{4}$$

for $i = 1, 2, 3, \cdots, N$, and

$$g_i(\alpha, V_l) = V_{l,i}^{-1}\{-V_{l,i}\sum_{k=0}^{N} V_k \mathbf{B}_{ik}\cos(\alpha_i - \alpha_k) - Q_{D,i}\} \tag{5}$$

with $i = m+1, m+2, m+3, \cdots, N$. In addition

$$f : \mathbb{R}^N \times \mathbb{R}^n \to \mathbb{R}^N, g : \mathbb{R}^N \times \mathbb{R}^n \to \mathbb{R}^n$$
$$\mathbf{\Pi} = [-\mathbf{e}|\mathbf{I}] = [\mathbf{\Pi}_1|\mathbf{\Pi}_2], \mathbf{\Pi}_1 \in \mathbb{R}^{N\times(m+1)}, \mathbf{\Pi}_2 \in \mathbb{R}^{N\times n}$$
$$\mathbf{e} = [-1, -1, \cdots, -1]^T, \mathbf{e} \in \mathbb{R}^N$$
$$\mathbf{D}_v \in \mathbb{R}^{n\times n}, P^0 = [P_1^0, P_2^0, \cdots, P_N^0]^T \in \mathbb{R}^N, Q_D \in \mathbb{R}^n$$

$\mathbf{M}_g$, $\mathbf{D}_g$, $\mathbf{D}_l$, $\mathbf{D}_v$ are constant diagonal matrices describing system parameters. $\mathbf{B}$ is the system's admittance matrix. Unlike reduced network models, this model does not decrease the dimension of the state space.

Implicit assumption lying in (4) and (5) is $\sum P_i = 0$, i.e. $\mathbf{G}_{ij} = 0$. However, we do not intend to assume the system as lossless. Instead, this system is assumed to have constant transmission loss during a short duration of time of interest. For each transmission line, the loss is calculated at steady state and then distributed evenly to the two connected bus nodes. This may result in $1\% \sim 5\%$ increase at load buses in a transmission system.

If we integrate the composite vector function $[(\mathbf{M}_g\omega_g)^T, f^T(\alpha, V_l), g^T(\alpha, V_l)]$ along a path from $x^0 = (\mathbf{0}, \alpha^0, V_l^0)$ to $x = (\omega, \alpha, V_l)$, we may have

$$\Phi(x, x^0) = \int_{\mathbf{0},\alpha^0,V_l^0}^{\omega_g,\alpha,V_l} [(\mathbf{M}_g\lambda)^T, f^T(\xi,\mu), g^T(\xi,\mu)] \cdot [d\lambda^T, d\xi^T, d\mu^T]^T \tag{6}$$

Here Φ represents the power system energy function. If we neglect the constant offset induced by x^0 from integration, we may simplify the form of Φ in general as

$$\Phi(x) = \frac{1}{2}\omega_g^T\mathbf{M}_g\omega_g - \frac{1}{2}\sum_{i=0}^{N}\sum_{k=0}^{N}\mathbf{B}_{ik}V_iV_k\cos(\alpha_i - \alpha_k) + \sum_{k=m+1}^{N} Q_{D,k}ln(V_k) + \alpha^T P^0 \tag{7}$$

This article has been accepted for publication in a future issue of this journal, but has not been fully edited. Content may change prior to final publication. Citation information: DOI 10.1109/TSG.2016.2548082, IEEE Transactions on Smart Grid

Define matrix $\mathbf{A}$ that

$$\mathbf{A} = \begin{bmatrix} -\mathbf{M}_g^{-1}\mathbf{D}_g\mathbf{M}_g^{-1} & -\mathbf{M}_g^{-1}\mathbf{\Pi}_1^T & \mathbf{0} \\ \mathbf{\Pi}_1\mathbf{M}_g^{-1} & -\mathbf{\Pi}_2\mathbf{D}_l^{-1}\mathbf{\Pi}_2^T & \mathbf{0} \\ \mathbf{0} & \mathbf{0} & -\mathbf{D}_v^{-1} \end{bmatrix} \tag{8}$$

Note that $\mathbf{A}$ is the sum of a diagonal matrix of non-positive entries and a skew symmetric matrix. With these definitions the model in (1),(2) and (3) may be rewritten as

$$\dot{x} = \mathbf{A}\nabla\Phi(x) \tag{9}$$

with matrix $\mathbf{A}$ non-singular and negative semi-definite, i.e. the equilibria of (9) occurs only at those points where $\nabla\Phi(x) = 0$, and

$$\dot{\Phi} = \frac{\partial\Phi}{\partial x}\frac{\partial x}{\partial t} = [\nabla_x\Phi(x)]^T\mathbf{A}\nabla_x\Phi(x) \leq 0 \tag{10}$$

Moreover, by LaSalle's theorem with Φ as a candidate energy-like Lyapunov function, it may be proved in our model that the equilibrium is asymptotically stable with no trajectories having $\frac{d\Phi}{dt} = 0$, if the Hessian about such equilibrium is positive definite [19]. This model and its extension has been widely applied in power system cascading failure analysis [13], [20], voltage stability measuring [17] and power grid dynamic control [14]. In the next section, we will introduce a new dynamic performance model of motor stalling/tripping, based on the similar structure as illustrated in (9) and (10).

III. A New Dynamic Performance Model of Motor Stalling and Thermal Tripping

A. Approximating Current Interrupting Relays via Smooth State Transitions

As concluded in [7], "the performance model represents the effects of motor loads in the form of real and reactive power consumption at three different states: running, stalled, and trip-off". In other words, a reasonable dynamic performance model should be able to reflect the sequential transition of the three states.

Let us introduce λ and μ as the two binary variables, which have three combinations corresponding to the three states: running, stalled and trip-off. In specific, when motor is operating at normal condition, $\lambda = 0$ and $\mu = 1$; when a fault occurs in the power system and leads to motor stalling, $\lambda = 1, \mu = 1$ and motor draws considerable reactive power from the grid; when motor is tripped off by thermal protection, λ stays at 1 and μ changes from 1 to 0.

The goal here is to allow the power system dynamic model to be constructed from a gradient of a smooth function, yielding a set of continuous ordinary differential equations. Therefore, two switching functions are introduced to smooth the transition between 1 and 0 of variable λ and μ. One may find similar functions in [13], [20]. Let us define the switching function vector $\hat{\theta}(\lambda)$ as:

$$\hat{\theta}(\lambda) = [\hat{\theta}_1(\lambda), \hat{\theta}_2(\lambda), \cdots, \hat{\theta}_p(\lambda)]^T \tag{11}$$

with $\lambda \in \mathbb{R}^p$, $\lambda = [\lambda_1, \lambda_2, \cdots, \lambda_p]^T$, and in specific

$$\hat{\theta}_r(\lambda) \equiv 2[-e^{-20\lambda_r} + e^{-200\lambda_r} + e^{20(\lambda_r-1)} - e^{200(\lambda_r-1)} + 0.2] \tag{12}$$

with $r = 1, 2, \cdots, p$, $p \leq n$, while p is the number of load buses with air conditioner motors installed, and n represents the number of load buses in the power system. Similarly, another switching function for μ is defined as:

$$\theta_r(\mu) \equiv 2[-e^{-20\mu_r} + e^{-200\mu_r} + e^{20(\mu_r-1)} - e^{200(\mu_r-1)} - 0.2] \tag{13}$$

with $\mu \in \mathbb{R}^p$, $\mu = [\mu_1, \mu_2, \cdots, \mu_p]^T$. Readers may notice that both $\hat{\theta}(\lambda)$ and $\theta(\mu)$ are written as a vector-valued function of a vector argument — in other words, the Jacobian of $\hat{\theta}(\lambda)$ and $\theta(\mu)$ are purely diagonal. Figure 2 illustrates the general idea of the two switching functions.

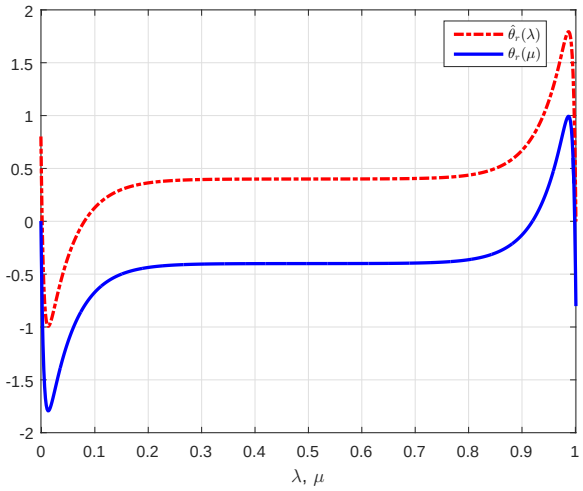

Fig. 2. Illustrative Plot of $\hat{\theta}_r(\lambda)$ (red dashed) and $\theta_r(\mu)$ (blue solid)

It should be pointed out that both λ and μ possess "one way" property — which means, once λ changes from 0 to 1, it will never change back. For μ, once it changes from 1 to 0, it will stay around 0 thereafter. Since λ and μ both fit into continuous expression, we will then rephrase them from "binary variables" to "bi-stable variables". Now we briefly illustrate the "switching mechanism" and the "bi-stable" property via the ordinary differential equation (14), with $W(\eta) > 0$ and $R_{\mu,r} > 0$:

$$\dot{\mu}_r = -D_{\mu,r}^{-1}(W(\eta) - R_{\mu,r}\theta_r(\mu)) \tag{14}$$

In this equation $R_{\mu,r}$ represents a pre-set threshold for $W(\eta)$. $D_{\mu,r}$ is a small positive time constant. Here η can be any state variable, e.g. load bus voltage, line current or frequency deviation, etc.. At normal operating point $\mu_r \approx 1$ and $R_{\mu,r}\theta_r(\mu) \approx R_{\mu,r} > W(\eta)$. Then suppose a fault occurs in the system and drives $W(\eta) > R_(\mu, r)$. From (14), such fault may activate the switching of variable μ_r by turning $-D_{\mu,r}^{-1}(W(\eta) - R_{\mu,r}\theta_r(\mu))$ negative, and push μ_r decreasing quickly from 1. Figure 2 indicates that $\theta_r(\mu)$ rises exponentially when μ_r drops below 0. Once $\theta_r(\mu)$ becomes large enough, $W(\eta) - R_{\mu,r}\theta_r(\mu) < 0$, then the right hand side of the equation (14) will become positive and μ_r will increase. However, in this example $W(\eta)$ will never become negative, therefore μ_r will stay a little below 0 thereafter, and $\mu_r \approx 0$.

This article has been accepted for publication in a future issue of this journal, but has not been fully edited. Content may change prior to final publication. Citation information: DOI 10.1109/TSG.2016.2548082, IEEE Transactions on Smart Grid

Similar to (6) and (7), the integral of this function proves important in our model development. The integral of a component $\theta_r(\lambda)$ with respect to λ is denoted as $\Theta_r(\lambda)$, as defined in (15). Similarly we have definition for $\hat{\Theta}_r(\mu)$ in (16). Both of the functions construct part of the energy-like Lyapunov function of the system, as shown in (30).

$$\hat{\Theta}_r(\lambda_r) \equiv \int_1^{\lambda_r} -\hat{\theta}_r(\eta)d\eta_r \tag{15}$$

$$\Theta_r(\mu_r) \equiv \int_1^{\mu_r} -\theta_r(\eta)d\eta_r \tag{16}$$

The following subsection will introduce how the two bistable variables λ and μ are incorporated into the dynamic performance model of motor loads.

B. Dynamic Performance Model for Motor Loads

Lawrence Berkeley National Lab published a detailed report regarding load and transmission modeling study in 2010 [6]. In this report, researchers investigated both the static performance model and the dynamic phasor model of air conditioner motor loads. For the static performance model, the experimentally observed motor $P-V/Q-V$ curve was fitted by the following representation for a single machine:

$$\begin{cases} P_{run} = a_1 + \frac{a_2}{V-a_0} + a_3(V-a_0) + a_4(V-a_0)^4 \\ P_{stall} = K_{P_1}V^3 + K_{P_2}V^2 \end{cases} \tag{17}$$

$$\begin{cases} Q_{run} = b_1 + \frac{b_2}{V-b_0} + b_3(V-b_0) + b_4(V-b_0)^4 \\ Q_{stall} = K_{Q_1}V^3 + K_{Q_2}V^2 \end{cases} \tag{18}$$

with a, b, K all real constants. P_{run}/Q_{run} stands for motor in operation, and P_{stall}/Q_{stall} stands for motor stalled.

As part of the project conducted in [6], researchers from Pacific Northwest National Lab also observed that the $P-V/Q-V$ trajectory of motor stall could be simplified as (19) in the aggregated model [21]:

$$P = K_P V^2, Q = K_Q V^2 \tag{19}$$

with K_P, K_Q real constants.

The P-V and Q-V relationship in (19) inspires us to develop an interesting model for motor stalling and tripping, from the following observations:

- Local low voltage may result in motor stalling
- The fitted curve reveals that the excessive drawing of reactive power on the load bus can be treated as the increment of shunt-inductor
- Most motors will be tripped due to the thermal protection after certain amount of time ($3 \sim 20$s)
- λ and μ can be incorporated into the dynamic performance model as indicator variables of state transition

Let us renumber the index for load buses: suppose buses numbered $m+1, m+2, \cdots, m+p$ have the aggregated model installed, $p \leq n$. Define vector $V_{lp} = [V_{m+1}, V_{m+2}, \cdots, V_{m+p}]^T$ as a subset of V_l. Based on those observations, the model can be constructed as

$$\begin{aligned} \dot{\lambda} = &-\mathbf{D}_\lambda^{-1}((\frac{1}{2}K_1 \circ \mu) \circ (V_{lp} \circ V_{lp}) + K_2 \circ T \\ &- K_\lambda - R_\lambda \circ \hat{\theta}(\lambda)) \end{aligned} \tag{20}$$

$$\begin{aligned} \dot{\mu} = &-\mathbf{D}_\mu^{-1}(\frac{1}{2}(K_1 \circ \lambda) \circ (V_{lp} \circ V_{lp}) \\ &+ K_3 \circ T - R_\mu \circ \theta(\mu)) \end{aligned} \tag{21}$$

$$\begin{aligned} \dot{T} = &-\mathbf{D}_T^{-1}(K_2 \circ \lambda + K_3 \circ \mu \\ &- K_T \circ (T - T_c)) \end{aligned} \tag{22}$$

while $\lambda, \mu, T, T_c, K_1, K_2, K_3, K_\lambda, K_T, R_\mu, R_\lambda \in \mathbb{R}^p$, except for $\mathbf{D}_{\lambda,\mu,T} \in \mathbb{R}^{p\times p}$. All Ks and all Rs are constants and T_c is a constant related to the armature ambient temperature:

$$T_{amb} = \frac{K_3}{K_T} + T_c \tag{23}$$

Here symbol $\circ$ represents the Hadamard Product: for vectors α and β have same length p,

$$\gamma = \alpha \circ \beta = [\alpha_1\beta_1, \alpha_2\beta_2, \cdots, \alpha_p\beta_p]^T \tag{24}$$

With (20), (21) and (22), the equation (3) is modified to yield:

$$\dot{V}_r = -D_r^{-1}\hat{g}_r(\alpha, V_l) \tag{25}$$

where

$$\begin{aligned} \hat{g}_r(\alpha, V_l) =& g_r(\alpha, V_l) + (K_{1,r} \circ \lambda_r) \circ (\mu_r \circ V_{l,r}) \\ =& V_{l,r}^{-1}\{-V_{l,r}\sum_{k=0}^{N} V_k \mathbf{B}_{rk}\cos(\alpha_r - \alpha_k) - Q_{D,r} \\ &+ (K_{1,r} \circ \lambda_r \circ \mu_r) \circ (V_{l,r} \circ V_{l,r})\} \end{aligned} \tag{26}$$

with $r = m+1, m+2, \cdots, m+p$.

To better understand how this model works, one may consider λ as "motor stalling indicator", μ as "motor operating indicator" and T as motor's armature temperature. It should be pointed out that the variable T is not designed to have a pure physical meaning. Instead, the variable T is implemented with motor operating indicator μ to mimic the inverse time-over current characteristic, as part of the motor's thermal protection.

When motor is operating normally, $\lambda = 0$, $\mu = 1$ and $T \approx T_{amb}$. Thus $(K_1 \circ \lambda) \circ (\mu \circ V_{lp}) = \mathbf{0}$ and (25) reduces to (3). If a to-ground fault swiftly pulls down the local voltage under a certain threshold, λ increases from 0 to 1, while μ remains unchanged. Then the motor stalls (refer to Table I) and draws a large amount of reactive power from the grid, i.e. (25) acts. During the motor stalling, the armature temperature T starts to increase and so does $K_3 \circ T$, the term that dominates the behaviour of motor operating indicator μ. After some time (21) is triggered, which drives μ falling from 1 to 0, i.e. motor trips. Readers may refer to Table I for more information regarding the roles of the different status of indicator variables.

In Table I, the motor tripping temperature T_{trip} is not explicitly shown in (22). Its value lies in the region

$$\frac{K_3}{K_T} + T_c < T_{trip} < \frac{K_3}{K_T} + T_c + \frac{K_2}{K_T} \tag{27}$$

since T_{trip} is reached when motor is stalling, i.e. $\lambda = 1$ and $\mu = 1$. If the motor stalls forever, then $T_{final} = \frac{K_3}{K_T} + T_c + \frac{K_2}{K_T}$. Therefore $T_{trip} < \frac{K_3}{K_T} + T_c + \frac{K_2}{K_T}$.

This article has been accepted for publication in a future issue of this journal, but has not been fully edited. Content may change prior to final publication. Citation information: DOI 10.1109/TSG.2016.2548082, IEEE Transactions on Smart Grid

TABLE I
VALUE OF PARAMETERS DURING DIFFERENT STAGES

	λ	μ	T
Operating Mode	0	1	T_{amb}
Transition Mode	$0 \rightarrow 1$	1	$T \uparrow$
Stalling Mode	1	1	$T \rightarrow T_{trip}$
Transition Mode	1	$1 \rightarrow 0$	$T \uparrow$
Tripping Mode	1	0	N/A

As part of a Lyapunov-based approach to power system cascading failure, the model presented in (20) $\sim$ (22) maintains a structure that allows it to be written in the form of

$$\dot{x} = \mathbf{A}_{ind} \nabla_x \Phi_{ind}(x) \tag{28}$$

Here the state vector $x = [\omega, \alpha, V_l, \lambda, \mu, T]^T$, and a negative semi-definite constant matrix $\mathbf{A}_{ind}$ is constructed as:

$$\mathbf{A}_{ind} = \begin{bmatrix} \mathbf{A} & \mathbf{0} & \mathbf{0} & \mathbf{0} \\ \mathbf{0} & -\mathbf{D}_{\lambda}^{-1} & \mathbf{0} & \mathbf{0} \\ \mathbf{0} & \mathbf{0} & -\mathbf{D}_{\mu}^{-1} & \mathbf{0} \\ \mathbf{0} & \mathbf{0} & \mathbf{0} & -\mathbf{D}_{T}^{-1} \end{bmatrix} \tag{29}$$

In particular, the energy-like Lyapunov function of motor stalling/thermal tripping model is constructed as

$$\begin{aligned} \Phi_{ind}(x) =& \frac{1}{2}\omega_g^T \mathbf{M}_g \omega_g - \frac{1}{2}\sum_{i=0}^{N}\sum_{k=0}^{N} \mathbf{B}_{ik} V_i V_k \cos(\alpha_i - \alpha_k) \\ &+ \sum_{k=m+1}^{N} Q_{D,k} ln(V_k) + \alpha^T P^0 + K_2^T (T \circ \lambda) \\ &+ \frac{1}{2}(K_1 \circ \lambda \circ \mu)^T (V_l \circ V_l) + K_3^T (T \circ \mu) - K_{\lambda}^T \lambda \\ &+ \mathbf{R}_{\lambda}^T \hat{\Theta}(\lambda) + \mathbf{R}_{\mu}^T \Theta(\mu) - \frac{1}{2} K_T^T (T \circ T) + K_T^T (T_c \circ T) \end{aligned} \tag{30}$$

Note that (30) satisfies (28), and one may determine $\nabla_x \Phi_{ind}(x)$ with (1), (2), (25) and (20) $\sim$ (22).

IV. CASE STUDY

In this section, IEEE 57 bus system is used to validate the feasibility of our model. The test case represents a simple approximation of the American Electric Power system in the Midwest. As shown in Figure 3, the system has 7 generators located outbound and 42 loads inbound. In particular, each load bus can be considered as an aggregation of a distribution network. For this study case, the aggregated dynamic performance motor models are installed on bus 38, 47, 50 and 53 respectively. As mentioned in the beginning of this paper, this model is developed to study the impact of FIDVR cascading from the distribution system through the transmission system. The simulation is carried out in MATLAB 2014b, and the full parameters for this simulation is provided in Table II.

If we illustrate the test set according to the three states of motor load:

1) Motor Operates Normally: When $t = 0$, the system was operating at steady state with all motor loads connected.
2) Motor Stall: Then at $t = 1.1s$, a resistor shunt fault $R_{fault} \approx 0.08 p.u.$ to ground was applied at bus 37 for 6 cycles (around 0.1 seconds) and then cleared. From Figure 4, one may see the motor loads at bus 38, 47 and 50 stalled sequentially soon after the fault occurred (i.e. λ changed from 0 to 1, as displayed in Table I). The stalled motor loads then induced large current, which led motor armature temperature T go up, as shown in Figure 5c. On the other hand, because of the long electric distance, the voltage of bus 53 changed little. The installed motor load still operates as usual (refer to

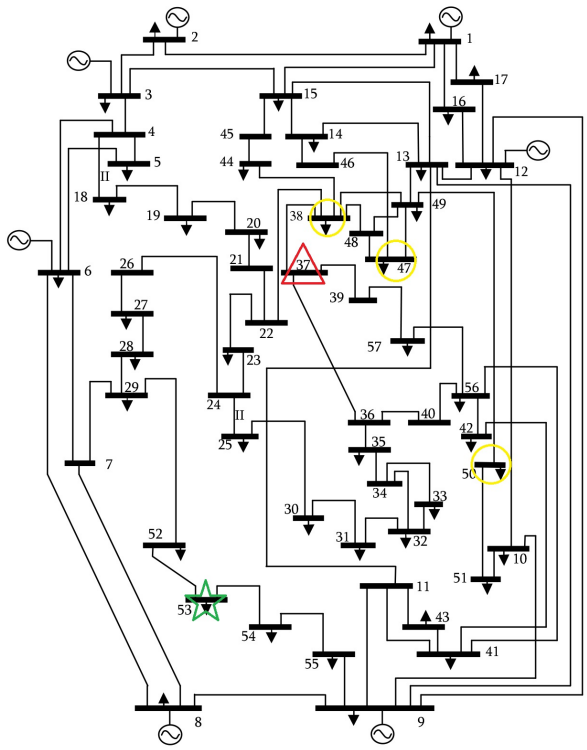

Fig. 3. Test Case on IEEE 57 Bus System: red triangle represents bus 37 has to-ground fault, yellow circles represent bus 38, 47 and 50 have motor stalled and tripped; green star represents bus 53 with motor not stalled

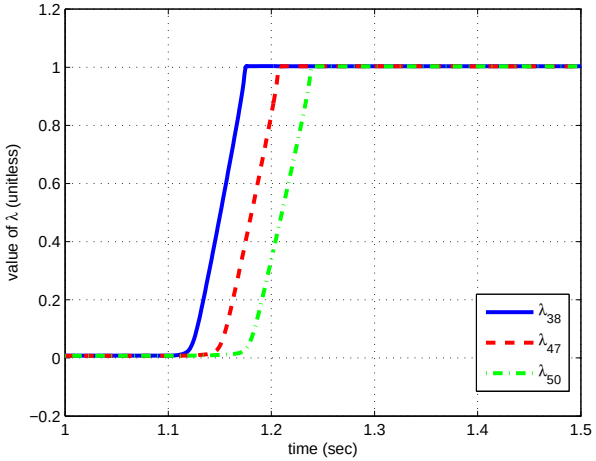

Fig. 4. Motor stalled consecutively when fault happens at $t = 1.1s$

This article has been accepted for publication in a future issue of this journal, but has not been fully edited. Content may change prior to final publication. Citation information: DOI 10.1109/TSG.2016.2548082, IEEE Transactions on Smart Grid

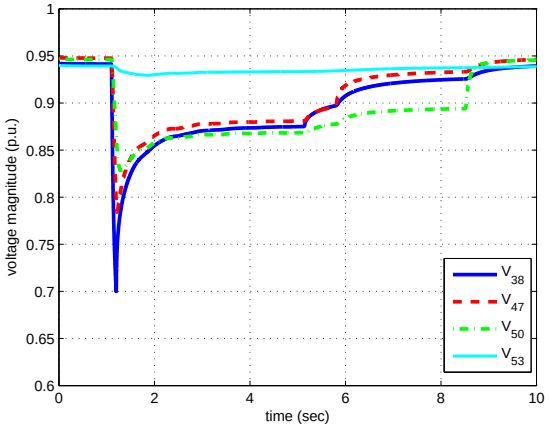

(a) Selected Voltage Plot (Bus 38, 47, 50, 53)

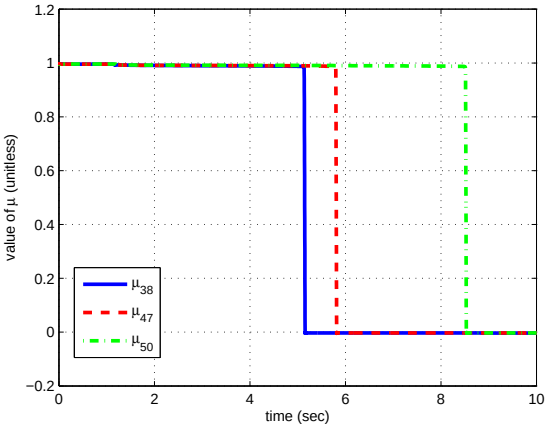

(b) Selected Indicator Plot (μ_{38}, μ_{47},μ_{50})

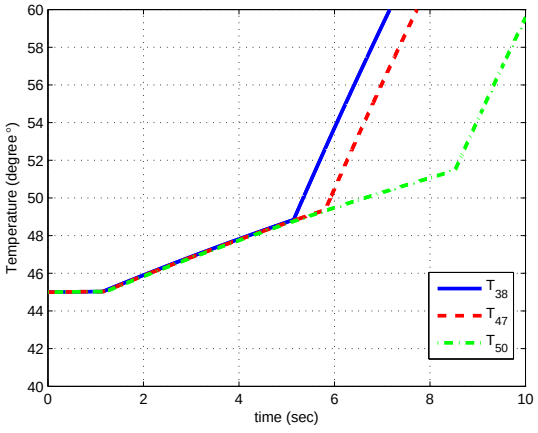

(c) Selected Temperature Plot(T_{38}, T_{47}, T_{50})

Fig. 5. Tested Model on IEEE 57 Bus System

Figure 5a) .

3) Motor Trip: After 3∼7 seconds, thermal protection acted ((22) and (21) together) to trip motor loads. μ, treated as "motor operating indicator", fell from 1 to 0 when temperature T reached a pre-set threshold. Since each motor load has a different pre-set T_{trip}, they were tripped at different time, as shown in Figure 5b.

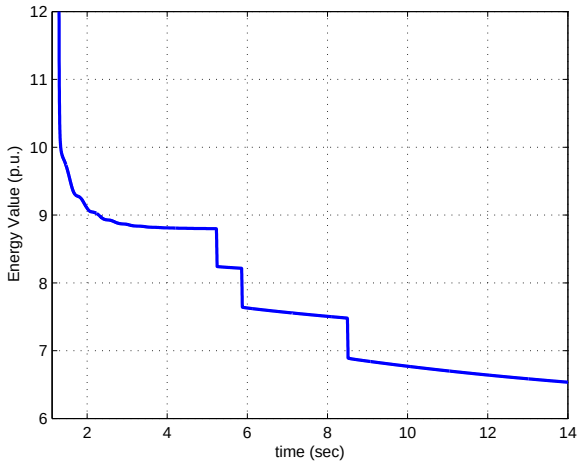

Fig. 6. $\Phi_{ind}(x)$ versus time t: energy goes down sharply at t=5.4s, 5.9s, 8.5s, from 8.9, 8.2 and 7.5, which corresponds to the tripping of motor loads on Bus 38, 47, 50.

As discussed previously, the variable T is not designed to possess a pure physical meaning. In this simulation, the motor armature temperature T still increases after disconnection of motor loads, as shown in Figure 5c. Therefore in Table I the "N/A" is used for T when motor trips from the grid. One may neglect the T trace after the motor is tripped off from the grid, since it will finally converge to a value.

Figure 5b shows the time for three motor loads on different bus to disconnect: 5.4s, 5.9s and 8.5s. If one plot the model associated energy-like Lyapunov function versus time, then the exact swift transition of the energy curve can be observed at the same time stamps. After these stepping-down changes, the energy value gradually converged and no more failure should be expected.

The plot in Figure 6 shows that the energy value is around 12 p.u. immediately after the fault, then quickly decreases. It stepped down at 5.4s, 5.9s and 8.5s with the energy 8.9, 8.2 and 7.5 p.u. respectively.

V. The Role of Relay Action in Setting Energy Thresholds

One of the key features associated with our smoothed model of motor stalling and relay actions is the fact that the dynamics associated with indicator variable transition inherently introduce a new class of unstable equilibrium points. In particular, consider the behaviour displayed in Figure 2. In the vicinity unity, as the value of operational value begins to move towards zero (the "failed" state), the energy term associated with the indicator variable encounters a sharp local maximum. While such a one-dimensional picture oversimplifies the true high-dimensional behavior, we claim that these dynamics typically create a type-1 unstable equilibrium point (u.e.p.), at which the Hessian of the energy function (i.e. $\nabla^2\Phi(x)$) has one negative eigenvalue, and all other eigenvalues positive. Intuitively, the one-dimensional plot of Figure 2 illustrates the behavior of the

This article has been accepted for publication in a future issue of this journal, but has not been fully edited. Content may change prior to final publication. Citation information: DOI 10.1109/TSG.2016.2548082, IEEE Transactions on Smart Grid

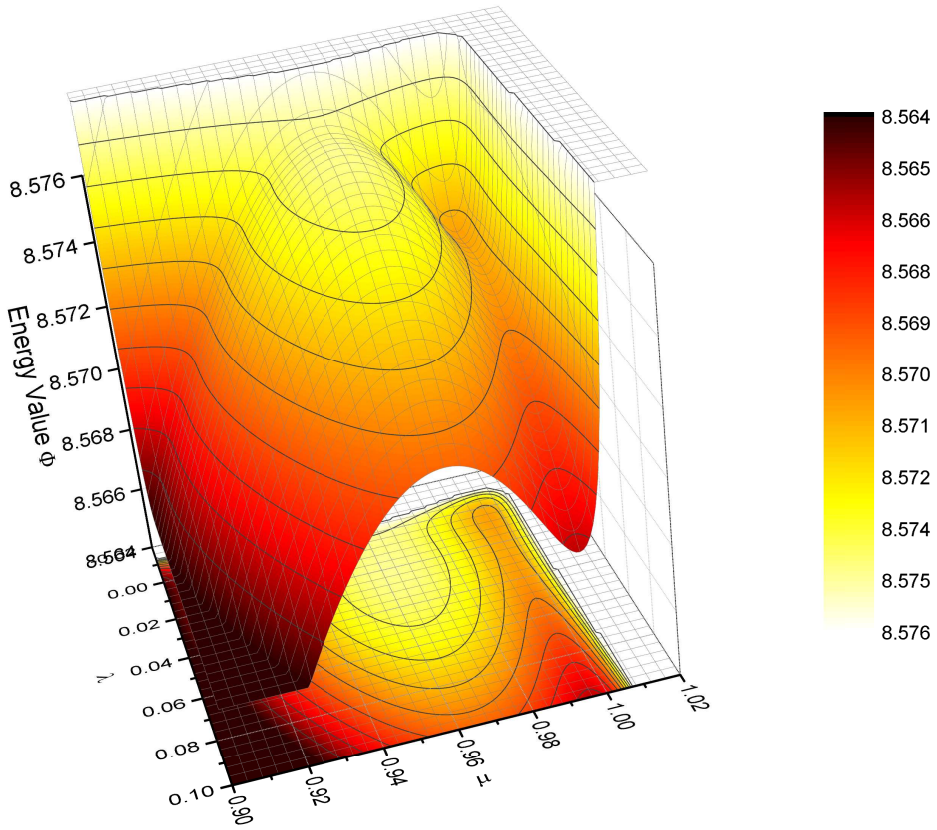

Fig. 7. 3D Plot of $\Phi_{ind}(x)$ with λ_{50} and μ_{50} two planar coordinate cut ($\lambda_{50} \approx -0.02 \sim 0.10$ and $\mu_{50} \approx 0.90 \sim 1.02$).

energy along the direction of the eigenvector associated with the one negative eigenvalue of the Hessian, which displays a sharp local maximum. Along all other eigen-directions, the energy is at a local minimum, consistent with the type-one u.e.p. It is the energy threshold at this "failure threshold" u.e.p. that must be overcome for this system to transition from normal operation, to the locally stable equilibrium of a stalled state; then another energy threshold at another u.e.p. must be overcome to further transition from the stalled state to the disconnect state. A cascading failure then represents a chain of such transitions.

The behavior of the energy function, which is projected onto the two coordinates λ_{50} and μ_{50}, is presented in Figure 7. A comparatively small measure for λ_{50} (-0.02 $\sim$ 0.10) and μ_{50} (0.90 $\sim$ 1.02) is selected to better capture system's behavior. In this plot, at ($\lambda_{50} \approx 0$, $\mu_{50} \approx 1$) exists a local stable equilibrium point with energy 8.576, representing the motor operating normally. There are type-1 u.e.p.s located at $(0, 0.95)$ and $(0.03, 0.99)$ respectively. In addition we have another type-2 u.e.p. with the highest energy value at $(0.02, 0.96)$. The energy value of u.e.p. $(0, 0.95)$ is lower than the u.e.p. $(0.03, 0.99)$, which means when a system is disturbed, it may likely flow a trajectory that will drive $\lambda = 0$ to $\lambda = 1$.

Note that $\lambda_{50} \approx 1$, $\mu_{50} \approx 1$ may be or not be a stable equilibrium, because of tripping temperature $T_{50,trip}$'s impact.

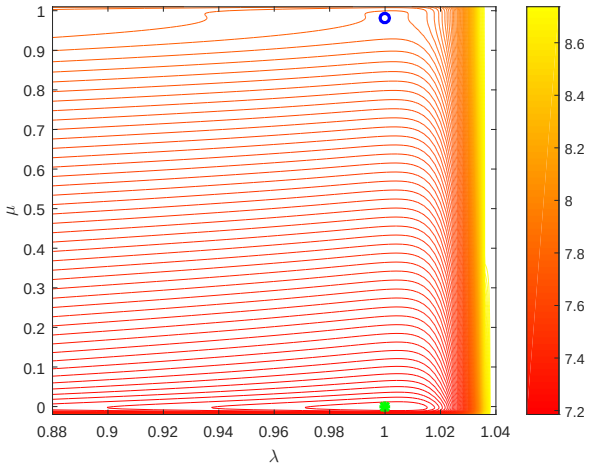

Fig. 8. 2D Plot for $\Phi_{ind}(x)$ with $\lambda_{50} \approx 0.88 \sim 1.02$ and $\mu_{50} \approx -0.02 \sim 1.02$

Here we select a case that $\lambda_{50} = 1, \mu_{50} = 1$ not representing a stable equilibrium state, as illustrated in Figure 8. As depicted in the plot, the system state at $\lambda_{50} \approx 1$, $\mu_{50} \approx 1$ is no longer a s.e.p., and the system state will finally converge to $\lambda_{50} \approx 1$,

$\mu_{50} \approx 0$, i.e. motor trip.

VI. Conclusion and Future Work

Understanding of the interplay between the individual component characteristic and system-wide phenomena it can induce is essential for smart grid monitoring and planning. In this work, we developed a new dynamic performance model of motor stalling and FIDVR phenomenon, aimed for potential applications within smart grid cascading analysis. Moreover, this model has a special structure that is closely related to the gradient of a scalar, energy-like function. With the incorporation of switching functions to mimic thermal relay action, it is easy to find the energy threshold type-1 u.e.p.s. We performed a testing case on IEEE 57 bus system to demonstrate the model's feasibility, and briefly illustrated the characteristics of the associated energy function.

For future work, this model can be further developed to incorporate power system dynamic control, to measure and mitigate the possibility of power system cascading failure. Moreover, it could be further tested with the commercial software to demonstrate its potential for practical application with smart control technology.

Appendix
Parameters Used in Section IV

The data of IEEE 57 standard system may be obtained from many sources. This work uses the case data from MATPower, an open-source software designed for research in transmission network analysis. For other important parameters please refer to Table II below:

TABLE II
Value of Parameters used in Section IV

2nd Order Generator Model			
M_g	0.0531	D_g	0.05
Time Constants			
D_l	0.005	D_v	0.4
D_λ, D_μ	0.01	D_T	0.001
Other Constants			
K_1	0.4	K_2	-0.001
K_3	0.005	T_c	-55
K_T	5×10^{-5}	K_λ	0.22
R_μ	$0.4 \sim 0.43$	R_λ	0.1

References

[1] "A technical reference paper for fault induced delayed voltage recovery," Transmission Issues Subcommittee and System Protection and Control Subcommittee, NERC, Tech. Rep., June 2009.

[2] C. Taylor and D. Erickson, "Recording and analyzing the july 2 cascading outage [western usa power system]," *IEEE Computer Applications in Power*, vol. 10, no. 1, pp. 26–30, Jan 1997.

[3] "Bibliography on load models for power flow and dynamic performance simulation," *Power Systems, IEEE Transactions on*, vol. 10, no. 1, pp. 523–538, Feb 1995.

[4] "Standard load models for power flow and dynamic performance simulation," *Power Systems, IEEE Transactions on*, vol. 10, no. 3, pp. 1302–1313, Aug 1995.

[5] A. M. Stankovic, B. C. Lesieutre, and T. Aydin, "Modeling and analysis of single-phase induction machines with dynamic phasors," *IEEE Transactions on Power Systems*, vol. 14, no. 1, pp. 9–14, Feb 1999.

[6] B. Lesieutre, R. Bravo, R. Yinger, D. Chassin, H. Huang, N. Lu, I. Hiskens, and G. Venkataramanan, "Final project report on load modeling transmission research," *CIEE Report*, March 2010.

[7] Y. Liu, V. Vittal, J. Undrill, and J. H. Eto, "Transient model of air-conditioner compressor single phase induction motor," *IEEE Transactions on Power Systems*, vol. 28, no. 4, pp. 4528–4536, Nov 2013.

[8] K. Tomiyama, J. Daniel, and S. Ihara, "Modeling air conditioner load for power system studies," *Power Systems, IEEE Transactions on*, vol. 13, no. 2, pp. 414–421, May 1998.

[9] H. Wu and I. Dobson, "Cascading stall of many induction motors in a simple system," *IEEE Transactions on Power Systems*, vol. 27, no. 4, pp. 2116–2126, Nov 2012.

[10] ——, "Analysis of induction motor cascading stall in a simple system based on the cascade model," *IEEE Transactions on Power Systems*, vol. 28, no. 3, pp. 3184–3193, Aug 2013.

[11] H. Bai and V. Ajjarapu, "A novel online load shedding strategy for mitigating fault-induced delayed voltage recovery," *IEEE Transactions on Power Systems*, vol. 26, no. 1, pp. 294–304, Feb 2011.

[12] M. Paramasivam, A. Salloum, V. Ajjarapu, V. Vittal, N. B. Bhatt, and S. Liu, "Dynamic optimization based reactive power planning to mitigate slow voltage recovery and short term voltage instability," *IEEE Transactions on Power Systems*, vol. 28, no. 4, pp. 3865–3873, Nov 2013.

[13] C. L. DeMarco, "A phase transition model for cascading network failure," *IEEE Control Systems*, vol. 21, no. 6, pp. 40–51, Dec 2001.

[14] J. Sun, H. Zheng, Y. Hu, and Y. Chai, "A direct method for power system corrective control to relieve current violation in transient with upfcs by barrier functions," *International Journal of Energy and Power Systems*, vol. 78, pp. 626–636, June 2016.

[15] N. Narasimhamurthi and M. R. Musavi, "A generalized energy function for transient stability analysis of power systems," *IEEE Transaction on Circuits Systems*, vol. CAS-31, no. 7, pp. 637–645, July 1984.

[16] A. R. Bergen and D. J. Hill, "A structure preserving model for power system stability analysis," *IEEE Transactions on Power Apparatus and Systems*, vol. PAS-100, no. 1, pp. 25–35, Jan 1981.

[17] C. L. DeMarco and T. J. Overbye, "An energy based security measure for assessing vulnerability to voltage collapse," *IEEE Transactions on Power Systems*, vol. 5, no. 2, pp. 419–427, May 1990.

[18] C. L. DeMarco and A. R. Bergen, "A security measure for random load disturbances in nonlinear power system models," *IEEE Transactions on Circuits and Systems*, vol. 34, no. 12, pp. 1546–1557, December 1987.

[19] M. Vidyasagar, *Nonlinear Systems Analysis*. Prentice-Hall, Inc. Englewood Cliffs, New Jersey, 1978.

[20] H. Zheng and C. L. DeMarco, "A bi-stable branch model for energy-based cascading failure analysis in power systems," in *North American Power Symposium (NAPS), 2010*, Sept 2010, pp. 1–7.

[21] N. Lu, Y. Xie, and Z. Huang, "Air conditioner compressor performance model," *PNNL Report*, August 2008.

Honghao Zheng received his B.S. degree from Huazhong University of Science and Technology in 2009 and M.S, Ph.D. degree in electrical engineering from University of Wisconsin - Madison, in 2011 and 2015 respectively. From July, 2015 he started working as a network application software engineer for SIEMENS in Minnetonka, Minnesota.

Christopher L. DeMarco holds the Grainger Professorship in Power Engineering and is Site Director for the National Science Foundation IUCRC Power Systems Engineering Research Center at the University of Wisconsin-Madison, where he been a member of the faculty of Electrical and Computer Engineering (ECE) since 1985. Dr. DeMarco received his PhD degree at the University of California, Berkeley in 1985, and his B.S. degree from the Massachusetts Institute of Technology in 1980, both in Electrical Engineering and Computer Sciences.